Genetic Algorithm-Driven Optimization of Multi-Tone Phase Modulation Signals for SBS Suppression in High-Power Fiber Amplifiers

Yulin Pan, Mengyue Shi, Weisheng Hu, and Lilin Yi

***Abstract*—To meet the demands of high-power, narrow-linewidth fiber lasers in defense and industrial applications, stimulated Brillouin scattering (SBS) has emerged as a critical bottleneck limiting power scaling. Conventional SBS suppression techniques, such as white noise and pseudo-random binary sequence (PRBS) modulation, often suffer from uncontrollable spectral broadening and limited tunability of the spectral shape. In this work, we propose a novel drive signal design methodology that leverages genetic algorithm (GA)-based optimization of frequency-domain amplitude distributions within a multi-tone modulation framework. This approach circumvents the randomness introduced by traditional binary modulation and enhances both the controllability and determinism of the signal. A simulation model based on the standard coupled three-wave and rate equations is utilized to systematically evaluate the impact of the optimized spectral profiles on SBS threshold enhancement. Simulation results demonstrate that, under a fixed 11 GHz of 20 dB RMS spectral bandwidth, the proposed scheme yields an SBS threshold improvement of approximately 400 W and 180 W over Gaussian-shaped and flat-top spectra, respectively. Experimental validation on a 2-kW-class fiber amplifier platform confirms these trends, with measured enhancements of 350 W and 120 W. These findings substantiate the feasibility and practical relevance of the proposed method, offering a new pathway for spectral engineering and SBS mitigation in next-generation high-power fiber laser systems.**

***Index Terms*—Narrow linewidth fiber amplifier, phase modulation, genetic algorithm, stimulated Brillouin scattering suppression.**

I. Introduction

TO MEET the stringent performance requirements imposed by defense, industrial, and medical applications, fiber lasers are expected to deliver ever-higher output power while maintaining excellent beam quality and narrow linewidth. However, power scaling in fiber lasers is fundamentally constrained by thermal damage, nonlinear effects, and modal instabilities [1], [2]. Under the condition of a limited spectral linewidth, the achievable output power reaches a ceiling, making the development of narrow-linewidth, high-power amplification systems a critical research focus. The master oscillator power amplifier (MOPA) architecture has gained widespread adoption due to its ease of control and effectiveness in scaling power. By seeding the amplifier with a stable, narrow-linewidth laser of a designated wavelength, substantial output power can be achieved through multi-stage amplification [3], [4].

Among the various nonlinear effects encountered during amplification, such as cross-phase modulation (XPM), stimulated Raman scattering (SRS), four-wave mixing (FWM), and stimulated Brillouin scattering (SBS)—SBS has the lowest threshold and is therefore the most easily triggered. As such, mitigating SBS is essential for further scaling the output power of fiber laser systems. Traditional approaches to SBS suppression include enlarging the effective mode area of the fiber [5], optimizing the pump configuration [6], [7], introducing gain competition [8], [9], and applying phase modulation to broaden the seed laser spectrum [10], [11]. Among these, spectral broadening via phase modulation stands out due to its structural simplicity and proven efficacy in SBS suppression, making it a prominent subject of ongoing research.

Spectral broadening of the seed source is typically achieved using a Mach–Zehnder phase modulator, which expands the linewidth of a single-frequency seed laser from the kilohertz to the gigahertz range. The spectral characteristics of the broadened signal are determined by the type of electrical drive applied to the modulator. Common drive signals include single-tone signals, white noise signals (WNS), and pseudo-random binary sequences (PRBS). Single-tone modulation is straightforward to implement but is limited in SBS suppression due to the finite bandwidth and microwave power handling capability [12]. WNS features a fully continuous spectrum, effectively reducing the power spectral density; however, it tends to generate random high-intensity pulses in the time domain, which can induce strong self-pulsing effects detrimental to power scaling [13]. PRBS, on the other hand, exhibit statistically balanced bit patterns, thereby avoiding time-domain spikes and offering better controllability than WNS. Nevertheless, their spectral envelope resembles a Gaussian shape rather than an ideal flat-top profile, which limits the maximum achievable SBS threshold [14], [15]. To address the limitations of these traditional modulation strategies, our research group has recently proposed a series of alternative phase modulation signals, including inversion probability-tuned waveforms [16], chirp-like signals optimized in the time domain [17], and binarized multi-tone signals [18].

Received 10 September 2025; revised 31 December 2025; accepted 14 January 2026. Date of publication 20 January 2026; date of current version 27 January 2026. This work was supported in part by the National Natural Science Foundation of China under Grant 62205198. *(Corresponding author: Mengyue Shi.)*

The authors are with the State Key Laboratory of Photonics and Communication, School of Electronic Information and Electrical Engineering, Shanghai Jiao Tong University, Shanghai 200240, China (e-mail: yulinpan@sjtu.edu.cn; sjtusmy@sjtu.edu.cn; wshu@sjtu.edu.cn; lilinyi@sjtu.edu.cn).

Digital Object Identifier 10.1109/JPHOT.2026.3656116

These novel approaches have demonstrated improved SBS suppression performance across multiple experimental evaluations, offering practical advantages over conventional schemes. Additionally, waveform optimization techniques—such as Pareto-based genetic algorithms—have been employed to refine time-domain modulation profiles [19]. However, these methods typically entail high-dimensional search spaces, resulting in substantial computational overhead and limited practical feasibility.

To the best of our knowledge, previous SBS suppression studies have primarily focused on time-domain waveform optimization or empirically designed frequency-domain spectra, while the direct optimization of frequency-domain spectral characteristics using an optimization algorithm—together with experimental validation—has not been systematically explored. By reformulating SBS suppression as a frequency-domain spectral optimization problem, the present work establishes a new framework that bridges deterministic spectral parameterization, physical modeling, and experimental verification. Although the optimization is shifted from the time domain to a more structured frequency-domain representation, the resulting problem remains nonlinear and non-convex, and the objective function is evaluated through a coupled physical model without explicit gradient information. In this context, a Genetic Algorithm (GA) is adopted due to its population-based global search capability, gradient-free nature, and flexible encoding, which naturally aligns with the proposed deterministic frequency-domain parameterization and enables efficient exploration of the reduced yet still nontrivial parameter space.

This study introduces a refined method that mitigates the randomness introduced by binarization through the deterministic encoding of the frequency-domain characteristics of the drive signal. A power amplification simulation model, incorporating both the three-wave coupling equations and rate equations, is employed to evaluate and iteratively optimize the encoded spectral amplitudes using a genetic algorithm. Simulation results indicate that, compared to Gaussian and flat-top spectra generated by prior binarized multi-tone methods, the optimized modulation scheme improves the SBS threshold by approximately 400 W and 180 W, respectively. To validate the effectiveness of the proposed method, a 2-kW-class fiber amplification platform was developed, and the optimized signal was experimentally compared with previously established schemes. This system enabled the generation of spectrally broadened signals with a 20 dB RMS linewidth of approximately 11 GHz while the drive signal is generated by a 2.5 Gbps low-speed digital-to-analog converter (DAC). Experimental validation confirms these improvements, with measured power enhancements of 350 W and 120 W. This study proposes a refined frequency-domain optimization scheme that reduces parameter dimensionality and enhances optimization efficiency, offering improved SBS suppression in a more deterministic and hardware-friendly manner.

II. Principle

A. Spectral Characteristics of High-Order Phase-Modulated Signals

A single-frequency seed laser with an intrinsic linewidth on the order of kilohertz can be spectrally broadened to the gigahertz regime via phase modulation. This process effectively redistributes the optical power of a single narrow spectral line into hundreds of frequency components, substantially reducing the average spectral power density and thereby increasing the threshold for SBS. The spectral profile resulting from phase modulation is highly dependent on the characteristics of the electrical drive signal, which can be implemented in various forms. Theoretically, it has been shown that an ideal rectangular spectral shape maximizes the SBS threshold limit [20]. However, the analytical modeling of arbitrary phase-modulated signals is inherently complex. To establish a foundational understanding, we begin by analyzing the case of a single-tone modulation applied to a single-frequency seed, where the optical field E(t) and the electrical drive signal V(t) can be expressed as

$$E(t) = E_0 e^{j\omega_c t} \tag{1}$$

$$V(t) = V_0 \sin(\omega_m t + \varphi) \tag{2}$$

Here, E_0 denotes the amplitude of the single-frequency seed laser, and ω_c is its angular frequency. The parameters V_0, ω_m, φ represent the amplitude, angular frequency, and initial phase of the sinusoidal electrical drive signal, respectively.

This electrical signal is amplified by a radio-frequency power amplifier with a gain factor of N, and subsequently applied to a phase modulator with a half-wave voltage of V_π . According to the operating principle of the phase modulator, the resulting modulated optical field $E_{out}(t)$ can be expressed as:

$$E_{out}(t) = E_0 e^{j\left(\omega_c t + \pi N \frac{V_0}{V_\pi} \sin(\omega_m t + \varphi)\right)} \tag{3}$$

By applying the Fourier transform to (3) and utilizing the Bessel function expansion, the spectral distribution of the modulated optical field in the frequency domain, denoted as $\tilde{E}_{out}(\omega)$, can be expressed as

$$\tilde{E}_{out}(\omega) = E_0 e^{jn\varphi} \sum_{n=-\infty}^{\infty} J_n\left(\pi N \frac{V_0}{V_\pi}\right) \delta(\omega - n\omega_m - \omega_c) \tag{4}$$

here, $\delta(\cdot)$ denotes the Dirac delta function, and $J_n(\cdot)$ is the nth-order Bessel function of the first kind.

When a single-tone signal is used to drive the phase modulator, the number of generated spectral lines is inherently limited by both the modulation bandwidth and the achievable modulation depth. To address this limitation, our group previously proposed a binarized multi-tone modulation scheme [18], in which several single-frequency signals are combined and used as the electrical drive signal. This approach enables the generation of an approximately flat-top optical spectrum and significantly enhances the SBS threshold compared to single-tone modulation.

A multi-tone signal can be regarded as the superposition of multiple sinusoidal components. According to the theoretical derivation provided in [21], the spectral distribution of the phase-modulated optical signal can be obtained as follows. The general expression of the drive waveform $V_m(t)$ can be written as:

$$V_m(t) = \sum_{k=1}^{l} V_k \sin(\omega_k t + \varphi_k) \tag{5}$$

By analogy with the analysis of single-tone drive signals presented above, when the multi-tone signal is applied to drive the

phase modulator, the single-frequency laser experiences phase modulation and the resulting optical field can be expressed as:

$$\tilde{E}_{m-out}(t) = E_0 \exp(j\omega_c t)\cdot \prod_{k=1}^{l} \sum_{n_k=-\infty}^{\infty} J_{n_k}\left(j\pi N \frac{V_k}{V_\pi}\right) \exp(jn_k k\omega_m t) \exp(jn_k\varphi_k) \quad (6)$$

By taking the Fourier transform of (6), the frequency-domain representation of the modulated optical signal $\tilde{E}_{m-out}(\omega)$ can be obtained:

$$\begin{cases} \tilde{E}_{m-out}(\omega) = E_0\delta(\omega-\omega_c) * M_1(\omega) * M_2(\omega) \\ \cdots * M_l(\omega) \\ M_l(\omega) = \sum_{n=-\infty}^{\infty} J_{n_l}\left(\pi N \frac{V_l}{V_\pi}\right) \delta(\omega - n_l\omega_l - \omega_c) \\ e^{jn_l\varphi_l} \end{cases} \quad (7)$$

Equations (6) and (7) form a Fourier transform pair: (6) describes the time-domain optical field with amplitude information of individual sideband combinations (via Bessel function products), while (7) reveals the frequency positions of spectral components (via convolution of single-tone delta functions). Neither alone suffices to fully characterize the modulated spectrum: (7) cannot account for amplitude superposition of overlapping sideband combinations, and (6) does not explicitly show frequency distribution.

Thus, combining (6) and (7) enables rigorous derivation of both the frequency positions ($\omega = \omega_c + \sum_{k=1}^{l} n_k\omega_k$) and total amplitude coefficients of the spectral components. Specifically, the spectral components of the modulated optical field are located at $\omega = \omega_c + \sum_{k=1}^{l} n_k\omega_k$. In particular, the coefficient of the s-th sideband (with the carrier frequency defined as the 0-th order) is obtained by summing over all terms satisfying $\sum_{k=1}^{l} n_k = s$, which yields:

$$E_s = \sum_{\sum_{k=1}^{l} k\bullet n_k = s} E_0 \prod_{k=1}^{l} J_{n_k}\left(\pi N \frac{V_k}{V_\pi}\right) e^{jn_k\varphi_k} \quad (8)$$

Equation (8) expresses that the amplitude coefficient E_s at an arbitrary frequency point E_s after phase modulation is intrinsically related to the amplitude and phase of all higher-order harmonic frequency components of the electrical drive signal whose fundamental frequency equals E_s . To realize a rectangular optical spectrum, it is necessary for all sideband coefficients $\{E_i,\ i = 1, 2, 3\ldots\}$ to be equal. Although a unified expression has been derived to characterize the spectral sideband coefficients resulting from phase modulation, the stringent condition requiring all sideband coefficients to be identical typically renders the existence of a feasible solution unattainable.

Notably, the proposed multi-tone phase modulation scheme exhibits inherent robustness against frequency and phase instabilities of the drive signal, which is closely related to the spectral characteristics governing SBS suppression. From a physical perspective, small drifts in the drive frequencies ω_k primarily result in slight shifts in the positions of individual optical sidebands, while the overall spectral envelope (e.g., bandwidth, flatness) remains unchanged. Since SBS suppression performance is dominated by the maximum spectral peak formed by the superposition of multiple spectral components, rather than the exact positions of individual sidebands, moderate frequency fluctuations have a limited impact on the SBS threshold.

Regarding phase stability, phase perturbations of the drive signal mainly affect the instantaneous temporal waveform of the modulated optical field via sideband interference. However, such perturbations do not significantly alter the time-averaged power spectrum of the optical signal or the amplitude of the maximum spectral peak—both of which are the key factors determining SBS suppression. Thus, the proposed scheme demonstrates good robustness against phase noise of the drive signal in practical scenarios.

B. Power Amplification Model Based on Three-Wave Coupling and Rate Equations

The SBS effect can be regarded as a nonlinear interaction between the pump wave and the Stokes wave mediated by the acoustic field. Under a simplified framework, all interacting fields can be treated as slowly varying, linearly polarized envelopes, allowing the spatial evolution of the signal to be described using its envelope function [22].

In practical high-power fiber amplification systems, fiber coiling is typically employed to suppress higher-order modes. Accordingly, in the simulation analysis, it is assumed that only the fundamental mode propagates within the fiber. The relatively weak effects of self-phase modulation (SPM) and cross-phase modulation (XPM) are neglected. Based on the principle of three-wave coupling, in conjunction with the rate equations, a numerical model for fiber power amplification is established [23]:

$$\frac{dP_p}{dz} + \frac{1}{\nu_{gp}}\frac{dP_p}{dt} = -\alpha_p P_p - \Gamma_p\left[\sigma_a^p N - (\sigma_a^p + \sigma_e^p) N_2\right] P_p \quad (9)$$

$$\frac{\partial Q}{\partial t} + v_A \frac{\partial Q}{\partial z} = \left[\frac{\Gamma_B}{2} + i(\Omega_B - \Omega)\right] Q + i\kappa_2 E_P E_S^* + f \quad (10)$$

$$\frac{\partial E_S}{\partial z} + \frac{n}{c}\frac{\partial E_S}{\partial t} = -\frac{\alpha_s}{2}E_S + \frac{1}{2}\left[(\sigma_a^s + \sigma_e^s) N_2 - \sigma_a^s N\right] E_S + i\gamma_e\left(|E_S|^2 + 2|E_P|^2\right) E_S + i\kappa_1 E_B Q^* \quad (11)$$

$$-\frac{\partial E_B}{\partial z} + \frac{n}{c}\frac{\partial E_B}{\partial t} = -\frac{\alpha_s}{2}E_B + \frac{1}{2}\left[(\sigma_a^s + \sigma_e^s) N_2 - \sigma_a^s N\right] E_B + i\gamma_e\left(|E_B|^2 + 2|E_S|^2\right) E_S + i\kappa_2 E_S Q^* \quad (12)$$

$$\frac{\partial N_2}{\partial t} = -\frac{N_2}{\tau} + \frac{\Gamma_s\lambda_s}{hcA_{eff}}\left[\sigma_a^s N - (\sigma_a^s + \sigma_e^s) N_2\right](P_s + P_B) + \frac{\Gamma_p\lambda_p}{hcA_{eff}}\left[\sigma_a^p N - (\sigma_a^p + \sigma_e^p) N_2\right] P_p \quad (13)$$

In the above equations, the subscripts p, s, and B denote the pump light, signal light, and Stokes light, respectively. P represents the optical power, α is the fiber loss coefficient, and Γ denotes the overlap factor. σ_a and σ_e are the absorption and emission cross sections, respectively. E_s, E_B, and Q represent

TABLE I
KEY PARAMETERS AND THE VALUES USED FOR SIMULATION

λ_s	1062.43 nm	ρ_0	2210.0 kg/m^3
A_{eff}	3.53×10^{-10} m^2	T	293.15 K
n	1.45	v_A	5.897 × 10^3 m/s
N	6.52 × 10^{25} m^{-3}	τ	10 ns
k	1.3806 × 10^{-23} m^{2}kgs^{-2}K^{-1}	γ_e	0.902
L	9 m	ΔL	0.01 m

the normalized amplitudes of the signal light, Stokes light, and acoustic wave field, respectively. ν_{gp} is the group velocities of the pump, while γ_e is the electrostriction coefficient. Γ_B represents the acoustic damping rate, Ω_B is the acoustic resonance frequency while the Ω indicates the varied angular frequency. Other physical constants include the speed of light c, the effective doping concentration N, Planck's constant h, the acoustic velocity v_A and the core cross-sectional area A_c, τ denotes the mean lifetime of the upper state of Yb^{3+} ions.

The coupling between the optical and acoustic fields is characterized by two coefficients: $k_1 = \omega\gamma_e/2nc\rho_0$, $k_2 = \omega\gamma_e/2c^2 v_A A_{eff}$, where ω is the angular frequency of the optical wave, n is the refractive index, ρ_0 is the material density, and A_{eff} is the effective mode area [24].

The term $f(z,t)$ denotes the Langevin noise source, which accounts for thermally or quantum-mechanically induced acoustic fluctuations responsible for initiating the SBS process. It obeys the following statistical properties

$$\langle f(z,t) f^*(z',t')\rangle = Q_f \delta(z-z')\delta(t-t') \quad (14)$$

$$Q_f = \frac{2kT_0\rho_0\Gamma_B}{\nu_A^2 A_{eff}} \quad (15)$$

Here k is the Boltzmann constant and T_0 is the absolute temperature. This noise term characterizes the spontaneous scattering that seeds the SBS process in the fiber medium. The key simulation parameters are summarized in Table I.

The coupled three-wave and rate equations are numerically solved using the method of characteristics, in which the partial derivatives are transformed into ordinary differential equations along the characteristic lines $dz/dt = \pm c/n$. Following the approach described in [25], the equations are discretized and integrated step by step using a first-order scheme equivalent to the Euler method. A sufficiently small spatial step ($\Delta L = 0.01$m) is chosen to guarantee numerical stability and convergence of the solution.

Phase modulation effects are incorporated through the initial and boundary conditions of the optical field. Specifically, the input optical field at the fiber entrance is defined as $E_S(0,t) = E_S^0 \exp[j\phi(t)]$, where $\phi(t)$ denotes the applied phase modulation function and A_L^0 is the input field amplitude. At the initial time $t = 0$, the optical field inside the fiber is set to zero, i.e., $E_S(z>0,0) = 0$.

The Stokes wave is assumed to be counter-propagating with respect to the pump wave and is initialized to zero throughout the fiber at $t = 0$. It satisfies the boundary condition $E_B(L,t) = 0$,

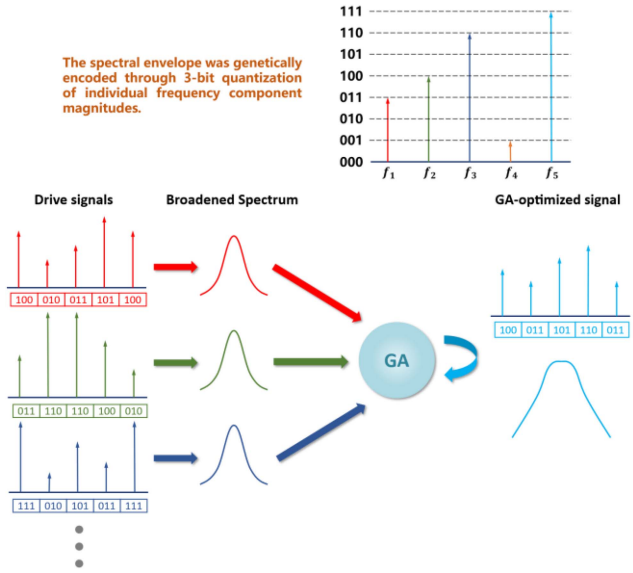

Fig. 1. Schematic of the amplitude encoding scheme.

following the standard SBS modeling approach reported in Ref. [25].

III. SBS THRESHOLD SIMULATION AND SPECTRAL PERFORMANCE ANALYSIS

A. Genetic Algorithm Design and Frequency-Domain Spectrum Optimization

To overcome the limitations associated with time-domain binarization and high-dimensional optimization, we propose a deterministic frequency-domain design strategy. By assigning distinct amplitude values to individual frequency components, the modulation signal avoids randomness and ensures a clear mapping between the electrical drive signal and the resulting optical spectrum. This approach significantly reduces the dimensionality of the optimization space, thereby improving computational efficiency and convergence stability. A schematic overview of the proposed design strategy is illustrated in Fig. 1. In addition, a quantization-based discretization method is introduced, where each spectral component is constrained to a finite set of amplitude levels $V = \{A^{(1)}, A^{(2)}, \ldots A^{(k)}\}$. This refinement transforms the original continuous optimization problem into a discrete one, further lowering complexity while enhancing practical feasibility for waveform implementation.

Within this framework, a genetic algorithm (GA) is employed to optimize the spectral amplitudes. Each individual is encoded as a vector $A = \{A_1, A_2, \ldots A_N\}$ where each element $A_k \in V$ corresponds to the amplitude of the k-th frequency component of the modulation signal. The decoding process reconstructs the spectral profile directly from A. For fitness evaluation, the constructed spectrum is incorporated into the coupled three-wave and rate-equation model, which is numerically solved using the method of characteristics along $dz/dt = \pm c/n$. The computed SBS threshold serves as the fitness function, ensuring that individuals yielding higher thresholds are preferentially selected.

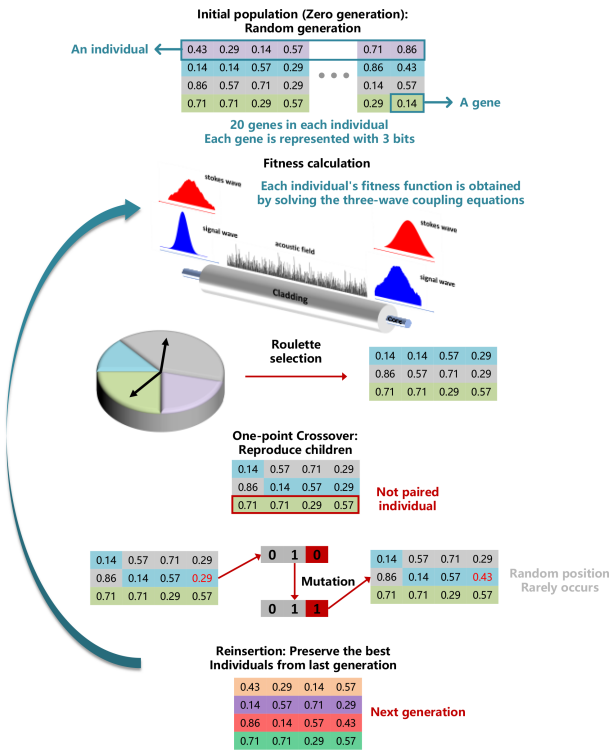

Fig. 2. Schematic diagram of spectral optimization using a genetic algorithm (GA).

B. Genetic Algorithm Optimization and SBS Threshold Simulation Results

To optimize the spectral shape of multi-tone electrical drive signals for enhanced suppression of stimulated Brillouin scattering (SBS), a genetic algorithm (GA) is integrated with a comprehensive simulation model of optical power amplification. In this model, the SBS threshold is defined as the forward output power corresponding to a backward (Stokes) signal level equal to 0.1‰ of the forward power. The drive signal design focuses on the amplitude configuration of discretized multi-frequency components. High-frequency tones primarily determine the phase-modulated spectral linewidth, while low-frequency tones shape the spectral envelope. An excess of low-frequency content typically results in a Gaussian-like distribution, which is less favorable for SBS suppression due to its power concentration in the spectral center.

To construct the multi-tone drive signal, 20 discrete frequency components are uniformly selected between 600 MHz and 790 MHz with a resolution of 10 MHz. Each amplitude value is quantized using 3-bit binary encoding, resulting in eight discrete levels per frequency point. This yields a chromosome length of 60 bits for each individual in the population. The encoding scheme reduces the search space while retaining sufficient resolution for effective spectral shaping. The complete procedure of the genetic algorithm is schematically depicted in Fig. 2.

The genetic algorithm begins with a randomly generated population. To ensure fair evaluation, all individuals are assigned the same set of random initial phases during optimization. The fitness function is defined as the SBS threshold calculated from the coupled three-wave and rate-equation model introduced in Section II. The SBS threshold P_{th} is defined as the input signal power at which the maximum backward Stokes power $E_B$reaches of 0.1‰ the forward power E_S, i.e.,

$$E_B\ (z\ =\ 0) = 1e^{-4} * E_S\,(z\ =\ L) \tag{16}$$

The GA optimization follows an iterative population-based process. An initial population is randomly generated within the predefined parameter ranges of the frequency-domain encoding. In each generation, all individuals are evaluated using the fitness function defined above, and the optimization proceeds iteratively until the termination criterion is satisfied. In each generation, A roulette-wheel selection strategy favors individuals with higher fitness scores, while single-point crossover recombines segments of two parent chromosomes with a probability of $p_c = 0.5$. Mutation is applied to individual gene values with a probability of $p_m = 0.05$, introducing stochastic variations that enhance diversity and help escape local optima. These parameter choices are consistent with commonly adopted ranges in GA-based optimization studies and were further validated through preliminary numerical tests, which confirmed that they provide a good balance between convergence speed and solution diversity in the present problem. Specifically, roulette-wheel selection is employed because the fitness value is a continuous scalar derived from numerical simulations, and a probabilistic selection pressure helps maintain population diversity during early generations. Single-point crossover is chosen since the chromosome represents an ordered set of frequency-domain parameters, and preserving contiguous gene segments is beneficial for maintaining physically meaningful spectral structures. The crossover probability $p_c = 0.5$ provides a balanced recombination rate that facilitates effective exploration without excessively disrupting well-performing solutions. The mutation probability $p_m = 0.05$ introduces controlled perturbations to avoid premature convergence while ensuring stable and computationally efficient optimization, considering the high cost of fitness evaluations. An elitism mechanism is also applied to retain the best-performing individual across generations, thereby improving convergence stability. Through this iterative process, the modulation spectra are autonomously evolved toward improved SBS suppression. The overall procedure is summarized in Fig. 2, where the direct integration of the physical model into the GA loop guarantees that the optimization remains physically meaningful.

The GA is configured with a population size of 100 and runs for 50 generations. The evolution of the maximum SBS threshold is illustrated in Fig. 3(a), where the optimized modulation spectrum leads to a power increase from 1580 W to 1860 W. In parallel, the spectral shape transitions from a Gaussian-like envelope to a flatter profile, as shown in Fig. 3(b).

To assess the relative effectiveness of the GA-optimized signal, SBS thresholds are compared with those of flat-top and Gaussian spectra under a fixed 20 dB RMS bandwidth of ∼11 GHz. These reference spectra are synthesized using the binary multi-frequency approach [17]. Phase modulation is applied using a half-wave voltage of V_π= 2.5 V, and signals are

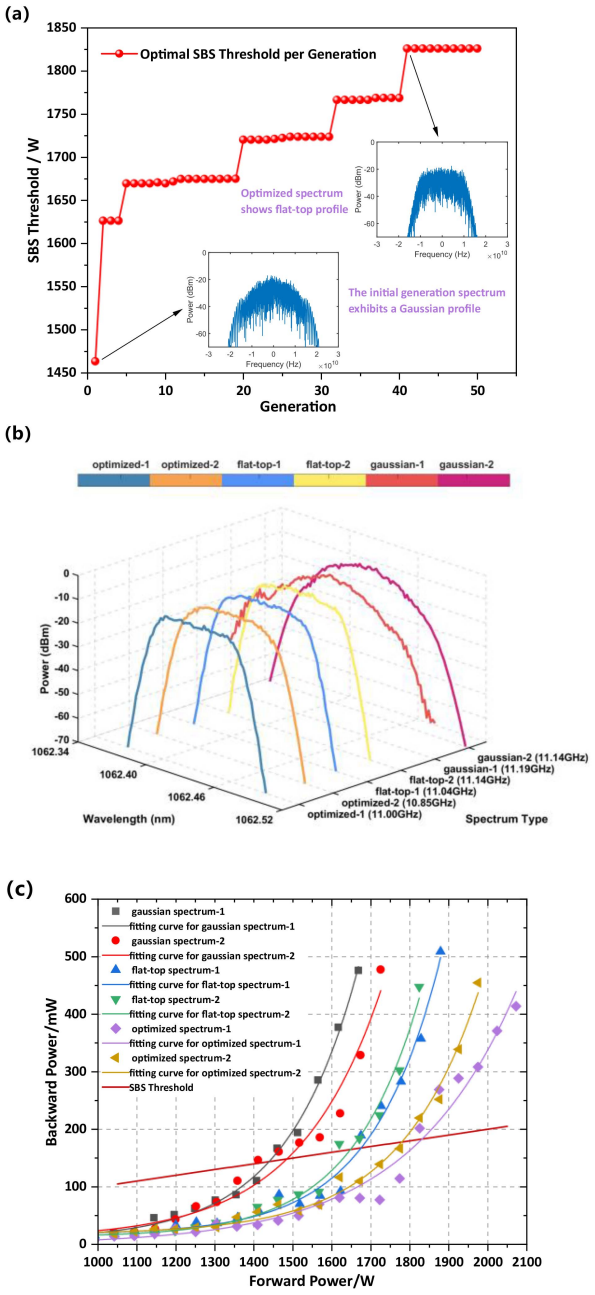

Fig. 3. (a) Evolution of the best fitness function values over 50 generations of genetic algorithm (GA) optimization. (b) Comparison of three drive schemes and their corresponding spectrally broadened outputs through phase modulation. (c) Comparison of amplified powers based on different driving signals.

sampled at 50 GSa/s. All spectra are bandwidth-equalized by adjusting drive power to ensure comparability. The resulting SBS thresholds, shown in Fig. (c), indicate that the GA-optimized spectrum outperforms the Gaussian and flat-top cases by approximately 400 W and 180 W, respectively.

The observed improvement in SBS threshold can be understood from the underlying physical mechanism of SBS, which is highly sensitive to local energy concentration and instantaneous power fluctuations. Spectra with narrow peaks or pronounced sidelobes tend to concentrate optical energy within limited spectral regions, which can induce self-pulsing behavior in the time domain and result in locally enhanced Brillouin gain, leading to premature SBS onset.

From this perspective, the GA-optimized spectrum exhibits several physically favorable characteristics. Compared with a Gaussian envelope, the flatter main lobe distributes optical power more uniformly over the frequency domain, effectively reducing local Brillouin gain through spectral averaging. The moderate spectral edges help suppress time-domain instabilities associated with abrupt spectral truncation, while the suppression of unwanted sidelobe peaks avoids excessive local energy concentration. These combined features mitigate SBS-triggering mechanisms and result in a higher SBS threshold.

This observation suggests that the GA not only maximizes the SBS threshold as an optimization objective, but also implicitly identifies spectral characteristics that are physically advantageous for SBS suppression.

IV. Experiment and Results

A. Experimental Setup

The experimental setup is illustrated in Fig. 4. In the spectral broadening module, a polarization-maintaining seed laser with a center wavelength of 1062.5 nm is employed as the seed source. The output light is first spectrally broadened by a phase modulator (PM), which is an iXblue device with a 2 GHz modulation bandwidth and a half-wave voltage of 2.5 V. The modulation signal is generated by a field-programmable gate array (FPGA) controlling a 2.5 GSa/s digital-to-analog converter (DAC) to produce the analog waveform. This signal is subsequently amplified by an electrical amplifier (EA) with a saturation output power of 33 dBm, and then used to drive the PM, enabling high-order phase modulation of the optical signal.

The spectrally broadened light is then injected into the master oscillator power amplifier (MOPA) module for power amplification. The MOPA consists of two stages of pre-amplification followed by a main amplifier. The seed signal passes through optical isolator ISO1, then into the first Yb-doped fiber pre-amplifier, which delivers an output power of 1.5 W. It subsequently passes through optical isolator ISO2 and into the second Yb-doped fiber pre-amplifier, which boosts the signal to 40 W. After the second pre-amplifier stage, the signal enters port 1 of an optical circulator (CIR). Port 2 is connected to the input of a mode field adapter (MFA), enabling efficient coupling into the main amplifier, while port 3 is used to extract the backward-propagating Stokes signal. The latter is directed to a photodetector (PD) and monitored in real time by a 10 GHz sampling oscilloscope (OSC) to observe the self-pulsing behavior associated with the SBS onset.

The main amplifier adopts a backward-pumping scheme using twelve 976 nm laser diodes (LDs), whose combined output—up to 2880 W—is delivered via a polarization-maintaining combiner (PMC) and injected from the rear end of the Yb-doped gain fiber. The gain medium is a commercially available PLMAYDF-20/400 polarization-maintaining large-mode-area fiber, supporting single-mode operation with a beam quality factor of $M^2 <$ 1.3. This configuration achieves an optical-to-optical efficiency

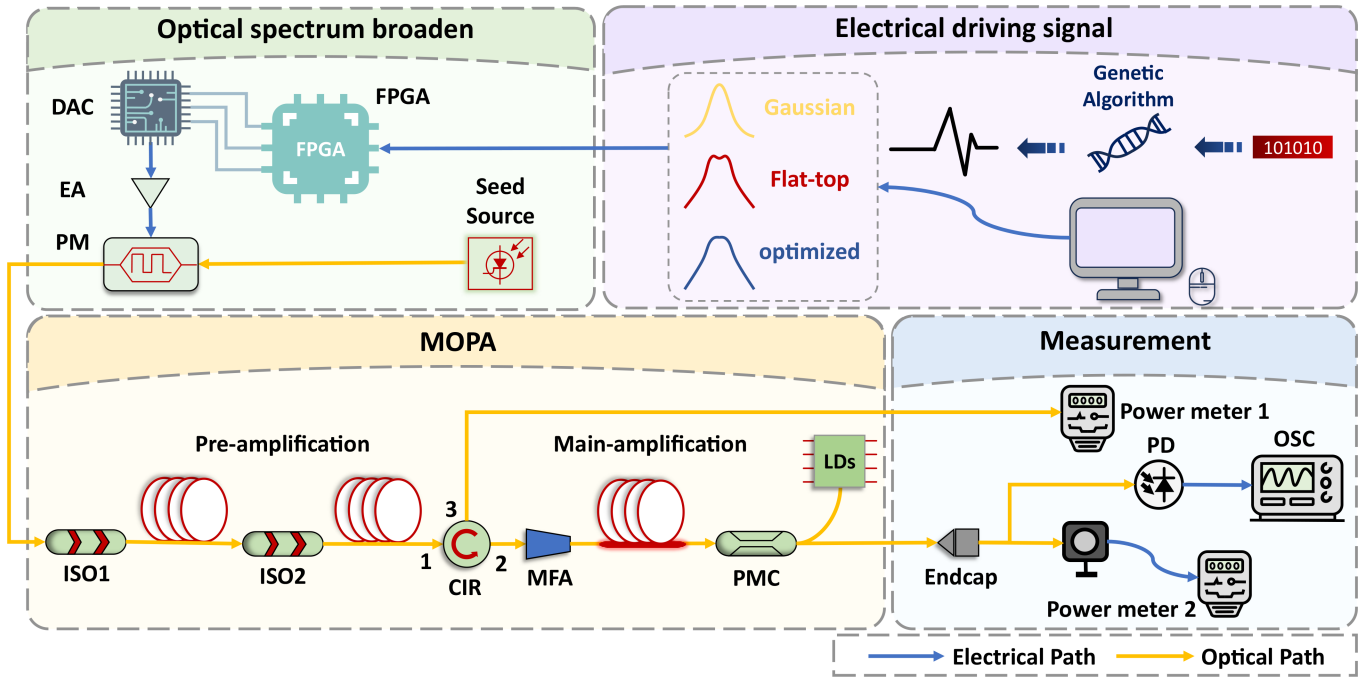

Fig. 4. The experimental setup of the spectral broadening module and the threshold measuring module. FPGA, Field Programmable Gate Array, DAC, digital-to-analog converter, LD, laser diode, EA, electrical amplifier, PM, phase modulator, ISO, optical isolator, CIR, optical circulator, PMC, polarization maintaining combiner, MFA, mode-field adapter, PD, photodetector, OSC, oscilloscope.

of ∼80%, with a maximum output power exceeding 2.3 kW. The amplified beam is emitted into free space through a fiber end-cap for safe high-power delivery, and the forward output power is measured using a high-power (>3000 W) optical power meter.

B. Experimental Results

To provide a fair comparison, several representative spectral shapes were constructed under the same 20-dB RMS linewidth constraint. The labels "Gaussian-1" and "Gaussian-2" correspond to Gaussian spectra generated with different random seeds in the discretization process, resulting in slightly different realizations while maintaining identical linewidths. Similarly, "flat-top-1" and "flat-top-2" denote flat-top spectra with small variations introduced to account for implementation differences. The "optimized-1" and "optimized-2" spectra are two distinct solutions obtained from independent GA runs starting with different initial populations. Both exhibit improved SBS suppression compared with the analytical spectra, but small differences in their detailed profiles demonstrate the stochastic nature of the GA search.

To experimentally validate the simulation results presented in Fig. 3, the six groups of drive signals were respectively loaded into the DAC to drive the phase modulator. By adjusting the DAC output power, the broadened optical spectrum maintained with an 20 dB RMS linewidth of approximately 11 GHz. A high-resolution optical spectrum analyzer with a frequency resolution of 30 MHz was employed to capture the spectral power distribution with sufficient detail for accurate comparison, as shown in (a). The SBS thresholds of the six modulated spectra were measured, as illustrated in Fig. 5(b). During the measurement process, both the forward and backward power levels were simultaneously recorded. Once self-pulsing behavior was detected by OSC, the measurement was immediately terminated to prevent equipment damage and ensure measurement reliability.

The two GA-optimized spectra - maintained their superior performance in experimental validation. The optimized spectrum with an 20 dB RMS bandwidth of 10.94 GHz achieved an SBS threshold of approximately 1705 W, representing an improvement of ∼120 W over the two flat-top spectra, whose bandwidths were 11.05 GHz and 11.32 GHz with corresponding thresholds of 1590 W and 1570 W, respectively. Compared to the Gaussian-shaped spectra with 20 dB RMS bandwidths of 11.07 GHz and 11.27 GHz, which yielded thresholds of 1370 W and 1330 W, the enhancement was around 350 W. These experimental results are consistent with simulation predictions, where the corresponding improvements were 180 W and 400 W, respectively.

The overall output power levels of the experimental power amplification platform were slightly lower than those predicted in simulations, which can be attributed to practical factors such as temperature fluctuations and fusion splice losses during the experiment. Moreover, discrepancies between the ideal phase modulation waveforms used in the simulation and the actual waveforms implemented on the physical platform may introduce additional inaccuracies. In particular, real-world device non-idealities—such as the frequency-dependent variation of the phase modulator's half-wave voltage and the harmonic suppression limitations of the electrical amplifier (EA)—can

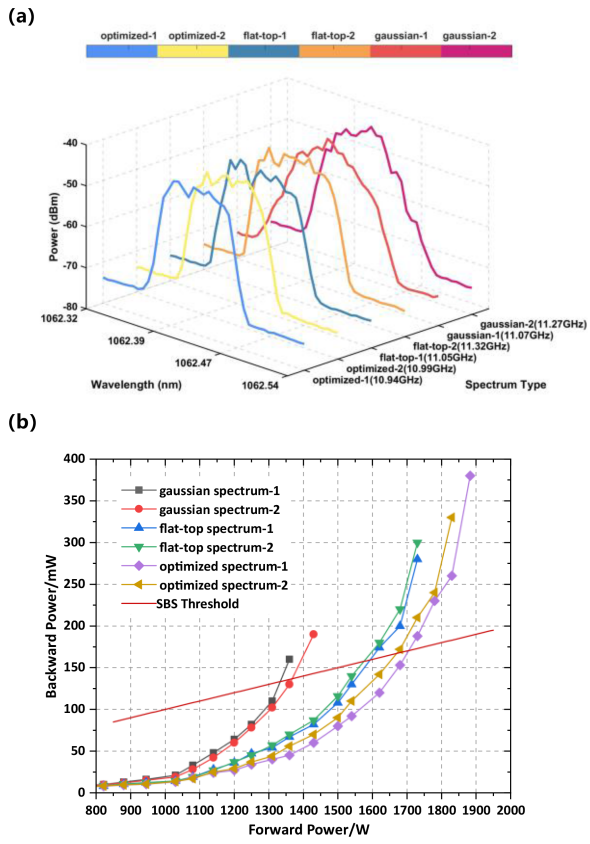

Fig. 5. (a) Measured broadened spectra of three drive schemes using a 30 MHz-resolution optical spectrum analyzer (b) Amplified power characteristics comparing GA-optimized spectrum, flat-top spectrum, and Gaussian spectrum in the experiment.

lead to waveform distortions that affect the SBS threshold measurement.

The GA-optimized spectral profiles consistently demonstrated superior SBS suppression performance over conventional spectral shapes across both simulated and experimental platforms. Despite minor discrepancies between simulation and experimental results due to hardware limitations, all driving signals were evaluated under consistent experimental conditions to ensure fair comparison. These findings highlight the practical viability of the proposed method for implementation in high-power fiber laser systems. Moreover, the framework established in this study provides a flexible basis for further exploration, such as extending the optimization to more complex spectral constraints, incorporating phase or polarization diversity, or jointly suppressing multiple nonlinear effects. This work offers new perspectives for intelligent spectral engineering in next-generation coherent and narrow-linewidth fiber amplifiers.

Although the genetic algorithm in this study is formulated as a single-objective optimization targeting the SBS threshold, other critical system-level performance metrics were also considered. Beam quality (M^2) in high-power fiber amplifiers is primarily governed by the fiber design, modal characteristics, pump configuration, and thermal effects, and the applied phase modulation operates purely in the temporal and spectral domains without introducing spatial perturbations or transverse mode coupling. As a result, no noticeable degradation in beam quality was observed, and the M^2 factor remained determined by the intrinsic properties of the fiber and pumping conditions. In addition, stimulated Brillouin scattering (SBS) and stimulated Raman scattering (SRS) arise from distinct physical mechanisms and exhibit substantially different threshold behaviors: SBS is a narrowband process with a relatively low threshold and typically represents the dominant limitation in narrow-linewidth high-power fiber amplifiers, whereas SRS is a broadband process with a significantly higher threshold under similar conditions. Therefore, SBS suppression is the primary concern in the present system. The optimized modulation bandwidth (∼11 GHz) is much smaller than the characteristic frequency shift associated with SRS, and no SRS onset was observed within the explored power range, indicating that the proposed scheme effectively suppresses SBS without inducing competing nonlinear limitations.

V. Conclusion

This work proposes and experimentally validates a spectral shaping method for SBS suppression based on genetic algorithm optimization in the frequency domain. To address the challenges of spectral uncertainty and parameter redundancy in traditional multi-tone modulation schemes, an amplitude quantization encoding strategy is developed, enabling a finite and efficient optimization space. Within a fiber amplifier simulation platform, the optimized modulation spectrum—with a 20 dB RMS linewidth of 11 GHz—yields a simulated SBS threshold enhancement of approximately 27% and 11% compared to Gaussian and flat-top spectra, respectively. Experimental validation on a 2-kW-class MOPA system confirms these trends, with measured threshold improvements of around 25% and 8%, closely aligning with simulation trends and confirming the method's practical viability. Given its robust adaptability, the proposed strategy can be extended to more complex spectral designs, multi-objective fitness optimization, and the co-suppression of other nonlinear effects, offering an intelligent and scalable solution for the next generation of high-power fiber laser systems.

References

[1] M. O'Connor, V. Gapontsev, V. Fomin, M. Abramov, and A. Ferin, "Power scaling of SM fiber lasers toward 10 kW," presented at the Conf. Lasers Electro-Opt., Baltimore, MD, USA, May 31–Jun. 5, 2009, Paper CThA3, doi: 10.1364/cleo.2009.ctha3.

[2] C. Jauregui, J. Limpert, and A. Tünnermann, "High-power fiber lasers," *Nature Photon.*, vol. 7, pp. 861–867, Dec. 2013, doi: 10.1038/nphoton.2013.273.

[3] A. Liem, J. Limpert, H. Zellmer, and A. Tünnermann, "100-W single-frequency master-oscillator fiber power amplifier," *Opt. Lett.*, vol. 28, no. 17, pp. 1537–1539, Sep. 2003, doi: 10.1364/OL.28.001537.

[4] L. Zhang, S. Cui, C. Liu, J. Zhou, and Y. Feng, "170 W, single-frequency, single-mode, linearly-polarized, Yb-doped all-fiber amplifier," *Opt. Exp.*, vol. 21, no. 5, pp. 5456–5462, Mar. 2013, doi: 10.1364/OE.21.005456.

[5] P. Ma, P. Zhou, Y. Ma, R. Su, X. Xu, and Z. Liu, "Single-frequency 332 W, linearly polarized Yb-doped all-fiber amplifier with near diffraction-limited beam quality," *Appl. Opt.*, vol. 52, no. 20, pp. 4854–4857, Jul. 2013, doi: 10.1364/AO.52.004854.

[6] C. Ren et al., "Investigation on SBS suppression in a kilowatt single-frequency-amplified Tm-fiber MOPA with distributed pumping," *Opt. Lett.*, vol. 50, no. 4, pp. 1200–1203, Feb. 2025, doi: 10.1364/OL.551700.

[7] Z. S. Eznaveh, G. Lopez-Galmiche, E. Antonio-Lopez, and R. A. Correa, "Bi-directional pump configuration for increasing thermal modal instabilities threshold in high power fiber amplifiers," *Proc. SPIE*, 2015, vol. 9344, Art. no. 93440M, doi: 10.1117/12.2080536.

[8] C. Zeringue, C. Vergien, and I. Dajani, "Pump-limited, 203 W, single-frequency monolithic fiber amplifier based on laser gain competition," *Opt. Lett.*, vol. 36, no. 5, pp. 618–620, Mar. 2011, doi: 10.1364/OL.36.000618.

[9] W. Lai, P. Ma, J. Song, S. Ren, W. Liu, and P. Zhou, "Kilowatt-level, narrow linewidth, polarization-maintained all-fiber amplifiers based on multi-phase coded signal modulation and laser gain competition," *Results Phys.*, vol. 31, 2022, Art. no. 10505, doi: 10.1016/j.rinp.2021.105050.

[10] M. Jiang, P. Ma, L. Huang, J. Xu, P. Zhou, and X. Gu, "kW-level, narrow-linewidth linearly polarized fiber laser with excellent beam quality through compact one-stage amplification scheme," *High Power Laser Sci. Eng.*, vol. 5, pp. e30, 2017, doi: 10.1017/hpl.2017.31.

[11] R. Prakash, B. S. Vikram, and V. R. Supradeepa, "Enhancing the efficacy of noise modulation for SBS suppression in high power, narrow linewidth fiber lasers by the incorporation of sinusoidal modulation," *IEEE Photon. J.*, vol. 13, no. 5, Oct. 2021, Art. no. 1500106, doi: 10.1109/JPHOT.2021.3111207.

[12] Y. Wang et al., "Effect of the recurring random signal waveform on SBS and self-pulsing in a phase-modulated narrow-linewidth linearly polarized fiber amplifier," *Opt. Commun.*, vol. 523, 2022, Art. no. 128683, doi: 10.1016/j.optcom.2022.128683.

[13] P. Ma et al., "High power all-fiberized and narrow-bandwidth MOPA system by tandem pumping strategy for thermally induced mode instability suppression," *High Power Laser Sci. Eng.*, vol. 6, pp. e57, Nov. 2018, doi: 10.1017/hpl.2018.51.

[14] C. Robin et al., "Pseudo-random binary sequence phase modulation in high-power Yb-doped fiber amplifiers," *Proc. SPIE*, vol. 8601, 2013, Art. no. 86010T, doi: 10.1117/12.2004486.

[15] Q. Shao et al., "Optimization of inversion probability tunable sequence phase modulation for SBS suppression in fiber system," *IEEE Photon. J.*, vol. 17, no. 2, Apr. 2025, Art. no. 1500812, doi: 10.1109/JPHOT.2025.3532907.

[16] M. Shi et al., "High-power narrow-linewidth fiber lasers using optical spectrum broadening based on high-order phase modulation of inversion probability-tuning sequence," *Opt. Exp.*, vol. 30, no. 6, pp. 8448–8460, Mar. 2022, doi: 10.1364/OE.449779.

[17] J. Li et al., "Spectral broadening scheme for suppressing SBS effects based on time-domain optimized chirp-like signals," *Opt. Exp.*, vol. 31, no. 5, pp. 8610–8621, Mar. 2023, doi: 10.1364/OE.483307.

[18] M. Shi et al., "High SBS threshold fiber laser with spectral management using binarized multi-tone signal modulation," *IEEE Photon. Technol. Lett.*, vol. 35, no. 9, pp. 513–516, May 2023, doi: 10.1109/LPT.2023.3249209.

[19] Y. Panbiharwala, A. V. Harish, Y. Feng, D. Venkitesh, J. Nilsson, and B. Srinivasan, "Stimulated Brillouin scattering mitigation using optimized phase modulation waveforms in high power narrow linewidth Yb-doped fiber amplifiers," *Opt. Exp.*, vol. 29, no. 11, pp. 17183–17200, May 2021, doi: 10.1364/OE.425159.

[20] A. V. Harish and J. Nilsson, "Optimization of phase modulation with arbitrary waveform generators for optical spectral control and suppression of stimulated Brillouin scattering," *Opt. Exp.*, vol. 23, no. 6, pp. 6988–6999, Mar. 2015, doi: 10.1364/OE.23.006988.

[21] K. Qu, S. Zhao, X. Li, Z. Zhu, D. Liang, and D. Liang, "Ultra-flat and broadband optical frequency comb generator via a single Mach–Zehnder modulator," *IEEE Photon. Technol. Lett.*, vol. 29, no. 2, pp. 255–258, Jan. 2017, doi: 10.1109/LPT.2016.2640276.

[22] C. Zeringue, I. Dajani, S. Naderi, G. T. Moore, and C. Robin, "A theoretical study of transient stimulated Brillouin scattering in optical fibers seeded with phase-modulated light," *Opt. Exp.*, vol. 20, no. 19, pp. 21196–21213, Sep. 2012, doi: 10.1364/OE.20.021196.

[23] W. Lai et al., "Seeding high brightness fiber amplifiers with multi-phase coded signal modulation for SBS effect management," *IEEE Access*, vol. 8, pp. 127682–127689, 2020, doi: 10.1109/ACCESS.2020.3007413.

[24] C. Zha et al., "Self-pulsing in kilowatt level narrow-linewidth fiber amplifier with WNS phase-modulation," *Opt. Exp.*, vol. 25, no. 17, pp. 19740–19751, Aug. 2017, doi: 10.1364/OE.25.019740.

[25] D. Hollenbeck and C. Cantrell, "Parallelizable, bidirectional method for simulating optical-signal propagation," *J. Lightw. Technol.*, vol. 27, no. 13, pp. 2140–2146, Jul. 2009, doi: 10.1109/JLT.2008.2009471.